Volume: 15 | Number: 01 | April 2026 | ISSN: 1907-4247 (Print) | ISSN: 2477-4863 (Online) | Journal Homepage: https://cantilever.id

Cantilever
Jurnal Penelitian dan Kajian Bidang Teknik Sipil

OPEN ACCESS

Research Article

Flexural and Shear Strength of RC Beam with Embedded Polystyrenes

Jen Hua Ling[1,*], Danson Tzet Lung Tan[1], and Yong Tat Lim[1]
[1]Centre for Research of Innovation and Sustainable Development, School of Engineering and Technology, University of Technology Sarawak, 96000 Sibu, Sarawak, Malaysia

Received: 8 January 2026, Accepted: 2 March 2026, Published: 25 June 2026

Abstract

This study examines the structural performance and material efficiency of reinforced concrete (RC) beams embedded with trapezoidal polystyrene, tested under flexural and shear loadings. The integration of polystyrene aims to reduce concrete volume while maintaining structural integrity. Twelve specimens were tested under four-point static loading, including five different polystyrene configurations and one control specimen for each loading type. Performance was evaluated based on load-displacement behavior, structural capacity, and material efficiency (i.e., strength gain vs concrete volume reduction). Results indicate that beams incorporating polystyrene remain functional. However, not all configurations increased load-bearing capacity; for example, PB5 showed decreased capacity. Performance is significantly influenced by the geometry of the embedded polystyrene, with increasing width having a more detrimental effect than depth. Among the specimens, PB2 exhibited the best overall performance, achieving 10% higher flexural capacity and 18% greater shear capacity despite a 10% reduction in concrete volume, resulting in 22% and 31% higher material efficiency under flexural and shear loadings, respectively. Some specimens, such as PB5, showed decreased capacity. These gains, however, were offset by lower cracking resistance and reduced ductility, which could limit the beam's serviceability and affect its suitability for structural applications requiring high deformation capacity or crack control. Despite its potential, the use of polystyrene in RC beams presents practical challenges, including the study's limited replication, construction complexity, and fire safety concerns, which must be addressed before broader implementation in structural applications.

Keywords: *concrete replacement, flexural and shear loading, lightweight concrete beam, material efficiency, polystyrene embedment.*

1. INTRODUCTION

The growing demand for lightweight beams stems from the need for more efficient, cost-effective, and sustainable construction. Reducing beam weight lowers dead loads, material use, foundation requirements, and overall costs, aligning with the UN Sustainable Development Goals (SDGs).

One approach is to embed polystyrene blocks within the reinforced concrete (RC) beam to create internal voids. Polystyrene is lightweight and inert, allowing for reduced self-weight without significantly altering the beam's shape or reinforcement. This method offers material savings while maintaining structural function.

Creating voids in beams is technically viable and aligns with classical beam theory, which assumes concrete in the tension zone provides minimal bending resistance [1]. However, this concrete is still needed to preserve section integrity and enable composite action.

Studies show mixed results. Some researchers report that lightweight beams can achieve higher load-carrying capacity despite reduced weight [2, 3]. Others find that capacity may decrease, but material efficiency improves [4, 5]. A few studies note a loss in overall performance [1, 6]. These contrasting findings highlight technical challenges that must be addressed before practical implementation.

Creating voids in beams changes their sectional properties and affects performance. Reducing the concrete area lowers stiffness and ductility [7, 8], causes uneven stress distribution, and leads to early cracking [9]. Voids also weaken shear and flexural capacities [8, 10, 11].

[5] found that void orientation, which affects the centroid, has little impact. The main concerns are reduced moment of inertia, which lowers bending

resistance [12], and reduced concrete area in shear resistance. [4] showed that placing polystyrene near supports weakens shear strength and leads to brittle failure. To address this, voids should be designed to limit their impact on bending stiffness and be kept away from high-shear regions.

Despite these findings, there is still no clearly defined method for systematically regulating void geometry and placement to preserve critical shear transfer zones while maintaining material efficiency. The lack of a geometry-based design approach limits the ability to balance weight reduction with structural reliability in voided RC beams.

Previous studies mainly used voids distributed along the full beam length in shapes such as spheres, cylinders, blocks, or pipes [1-5, 7, 10-14]. Earlier research reported that such voided beams reduced concrete volume by 8.4 to 11.8% and improved the strength-to-weight ratio [2, 3, 5, 12]. However, they focus mainly on flexural performance without addressing shear weaknesses near supports.

Instead of simply avoiding voids in high-shear regions, this study introduces a targeted void regulation strategy by aligning trapezoidal voids with expected shear crack paths, thereby preserving critical shear transfer zones while maintaining material reduction. This rationale forms the basis for developing trapezoidal voids with inclined faces positioned away from supports.

This study evaluates whether excluding voids along expected shear crack paths improves beam performance. Specifically, it investigates the influence of trapezoidal void width (B_p) and depth (D_p) on ultimate load (P_u), ductility, cracking behavior, and material efficiency under flexural and shear loading. The objective is to quantify how geometric variation affects structural capacity and efficiency, contributing to the development of optimized lightweight RC beams for sustainable construction.

2. METHOD

Specimen Details

This study tested twelve RC beams: six for flexure and six for shear, each group with one control beam. All beams were 1600 mm long, 175 mm wide, and 300 mm deep. The reinforcement included two 10 mm top bars, two 12 mm bottom bars, and 6 mm shear links spaced at 150 mm.

Specimen CB1 was the control beam, built using a standard RC design without polystyrene blocks. Specimens PB1 to PB5 had centrally placed trapezoidal polystyrene blocks with rectangular cross-sections (Figure 1). The key variables were block depth (D_p) and width (B_p) (Table 1). The trapezoidal profile had a fixed 45° angle, corresponding to the maximum diagonal concrete strut angle assumed in truss analogy models for shear reinforcement design [15].

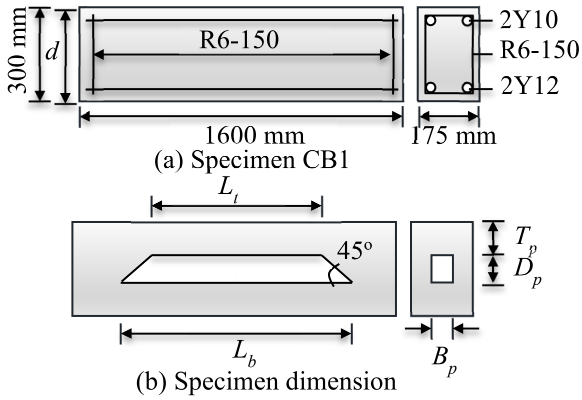

Figure 1. Details of specimens

In specimens PB1, PB2, PB4, and PB5, polystyrene blocks were placed 118 mm from the top surface (0.45*d*) to stay clear of the neutral axis during bending. This follows Eurocode 2 [16], which limits the neutral axis depth to 0.45*d* to ensure ductile failure by allowing the steel to yield before concrete crushes. Specimen PB3 used a deeper block (170 mm) placed 68 mm from the top (0.26*d*), extending into the compressive zone to study its structural effect.

It should be noted that each configuration was represented by a single specimen due to resource and time constraints; therefore, experimental variability and statistical dispersion could not be quantified.

Table 1. Details of polystyrene blocks embedded in specimens

Specimen	Polystyrene dimensions						Number of specimens	
	Top length, L_t (mm)	Bottom length, L_b (mm)	Inclined angle, θ (°)	Section width, B_p (mm)	Section depth, D_p (mm)	Section location, T_p (mm)	Flexural test (F)	Shear test (S)
CB1	-	-	-	-	-	-	1	1
PB1	1160	1300	45	60	70	118	1	1
PB2	1060	1300	45	60	120	118	1	1
PB3	960	1300	45	60	170	68	1	1
PB4	1060	1300	45	40	120	118	1	1
PB5	1060	1300	45	80	120	118	1	1

Notes: 118 mm and 68 mm correspond to 0.45*d* and 0.26*d*, respectively, where the effective depth (*d*) was 263 mm.

DOI: https://doi.org/10.35139/cantilever.v15i1.653

Table 2. Material specifications and conformity tests

Material	Specifications	Tests
Concrete	Ready-mix concrete, grade 25, designed slump 60 to 120 mm.	Compressive test and slump test
Steel reinforcement	High yield deformed bar, 10 mm and 12 mm diameters, yield strength 460 N/mm^2.	Tensile test
Shear link	Mild steel bar, 6 mm diameter, yield strength 250 N/mm^2.	Tensile test

Table 3. Material test

Material	Test	Equipment	No. of sample
Concrete	Compression test (BS EN 12390 – 3:2002)	Compressive Strength Machine (Brand: *ELE International*, Capacity 3000 kN)	2 units 150 mm samples per specimen
	Slump test (BS EN 12350 – 2:2009)	Slump Test Set	1 sample
Reinforcement and shear link	Tensile Test (ASTM A370)	Static Hydraulic Universal Testing Machine (Brand: *MTS*, Capacity 600 kN)	3 samples

Material Specifications

This study used ready-mixed concrete grade 25, steel reinforcement grade 460, and shear link grade 250, as detailed in Table 2. Cube compression and slump tests were carried out to confirm the concrete's strength and workability. Tensile tests on the reinforcement bars and shear links were conducted to determine their properties, as shown in Table 3.

Experimental Setup

All specimens were tested under four-point bending, as shown in Figure 2. Each beam was simply supported over a 1500 mm span using steel rocker supports. A hydraulic jack applied a static load through a steel I-beam, splitting it into two equal point loads.

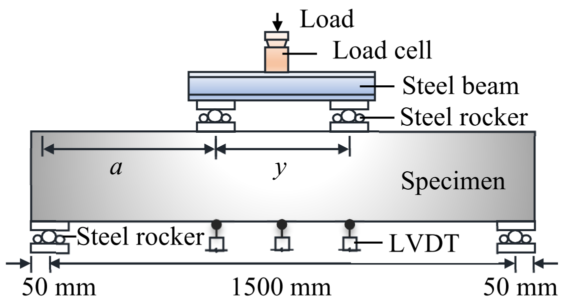

Figure 2. Test setup of specimen

Two loading setups were used:

1) Flexural loading: Point loads were 260 mm apart (approximately 1*d*) and centered at midspan (Table 4). Each was 620 mm from the supports (approximately 2.36*d*), creating a high bending moment at midspan with low shear near the supports.
2) Shear loading: Point loads were 800 mm apart (approximately 3*d*), with each 350 mm from the supports (approximately 1.3*d*). This setup increased the possibility of shear failure due to bending reduction at midspan.

Table 4. Location of point loads

Load case	Distance to Support, *a* (mm)	Distance Between Loads, *y* (mm)
Flexural load	620	260
Shear load	350	800

Load and displacement were recorded during testing. As shown in Table 5, a load cell measured the applied load, while three LVDTs measured deflection: one at midspan and two under each point load. All devices were connected to a data logger and computer for real-time monitoring of the load and displacement response.

Table 5. Instrument specifications

Equipment	Brand, Model	Description	Function	Data accuracy
Hydraulic Cylinder	*Enerpac*, RR-10018	Push capacity: +933 kN; Pull capacity: -435 kN	To apply controlled loading to the specimen	-
Hydraulic pump	*Enerpac*, P464	Max operating pressure: 700 bar	To supply hydraulic pressure to drive the loading system	
Load Cell	*TML*, CLJ-300KNB	Load capacity: 300 kN	To measure the applied load	0.01 kN
Displacement Transducer	*TML*, CDP-100	Measurement capacity: 100 mm	To measure the displacement of the instrumented point	0.01 mm
Data Logger	*TML*, TDS-530	30 input channels	To record signals from all sensors	-

DOI: https://doi.org/10.35139/cantilever.v15i1.653

Testing Process

Before testing, all instruments were zeroed. A preload up to 10% of the estimated capacity was applied for 5 minutes, then released for another 5 minutes to check if readings returned close to zero. This cycle was repeated twice to ensure the devices worked properly.

After the final zeroing, the test began. The load was increased in steps of 5 kN or 0.1 mm deflection, whichever came first. At each step, readings were taken after holding the load for at least one minute. Cracks were marked at each stage to track their growth. The test ended when five consecutive load readings dropped or a clear reduction in load capacity was observed.

3. RESULTS AND DISCUSSION

Material Properties

Table 6 shows the density, compressive strength, and slump values of concrete cubes cast with each beam. Slump values ranged from 155 mm to 160 mm, above the target range of 60 mm to 120 mm. The concrete remained workable and compacted well without segregation or bleeding, making it acceptable. Visual inspection during demolding indicated no honeycombing or surface defects, suggesting that workability remained acceptable for proper placement. All 28-day compressive strengths exceeded the 25 N/mm^2 design target, confirming concrete quality. Densities ranged from 2304 kg/m^3 to 2397 kg/m^3, consistent with normal-weight concrete and indicating no abnormal voids.

Table 6. Test results of concrete

Specimen	Density (kg/m^3)			Compressive stress (N/mm^2)			Slump (mm)
	Sample 1	Sample 2	average	Sample 1	Sample 2	average	
CB1(F)	2304	2325	2315	25.0	25.5	25.3	155
PB1(F)	2338	2329	2334	25.6	25.4	25.5	160
PB2(F)	2379	2397	2388	26.3	28.5	27.4	160
PB3(F)	2341	2382	2362	25.3	27.3	26.3	160
PB4(F)	2359	2373	2366	25.7	27.1	26.4	160
PB5(F)	2329	2385	2357	26.1	27.4	26.8	160
CB1(S)	2338	2329	2334	25.6	25.4	25.5	160
PB1(S)	2344	2376	2360	25.4	26.9	26.2	160
PB2(S)	2359	2373	2366	25.7	27.1	26.4	160
PB3(S)	2329	2385	2357	26.1	27.4	26.8	160
PB4(S)	2379	2397	2388	26.3	28.5	27.4	160
PB5(S)	2329	2385	2357	26.1	27.4	26.8	160

Although minor variations in compressive strength and density were observed among the 28-day concrete cubes tested on the day of specimen loading, all were cast from the same ready-mix batch. The measured values fell within a narrow range and exceeded design targets, indicating negligible influence on the comparative analysis of specimen performance.

Table 7 shows the steel reinforcement met standards, with tensile strengths over 460 N/mm^2 for main bars and over 250 N/mm^2 for shear links. Overall, the material properties met specifications, reducing the risk of results being influenced by poor-quality materials.

Table 7. Tensile strength of steel bars (N/mm^2)

Steel Bar	Sample 1	Sample 2	Sample 3	Mean
Y12	531	670	660	620
Y10	590	640	635	622
R6	290	279	285	285

Notes
Y12 and Y10 denote steel reinforcement bars with diameters of 12 mm and 10 mm, respectively, whereas R6 denotes shear links with a diameter of 6 mm. Tensile strengths are in N/mm^2.

Geometrical Properties

Embedding polystyrene within the specimen reduces the volume of concrete, V_c, which is calculated by subtracting the volume of the embedded polystyrene, V_p, from the total beam volume, V_b, as shown in Equation (1):

$$V_c = V_b - V_p \quad (1)$$

The total volume of the RC beam, V_b, is determined using Equation (2):

$$V_b = LBH \quad (2)$$

where L, B, and H represent the beam's length, width, and height, respectively (in mm). Given: L = 1600 mm, B = 175 mm, H = 300 mm.

The volume of the embedded trapezoidal polystyrene block, V_p, is calculated using Equation (3):

$$V_p = \frac{1}{2}(L_t + L_b)B_pD_p \quad (3)$$

where L_t and L_b are the top and bottom lengths of the trapezoidal polystyrene block (mm), B_p is the width of the polystyrene block cross-section (mm), and D_p

is the height of the polystyrene block cross-section (mm).

The percentage of concrete volume replaced by polystyrene, V_r, is given by:

$$V_r = \frac{V_p}{V_b} \times 100\% \quad (4)$$

This shows how much of the beam volume is occupied by polystyrene. In this study, up to 13.7% of concrete volume was replaced, as shown in Table 8. Since polystyrene weight is negligible, this also reflects the weight reduction of the specimen [12].

Table 8. Percentage of concrete replacement by polystyrene embedded in the specimens

Specimen	Volume of polystyrene, V_p (mm^3)	Volume of beam, V_b (mm^3)	Concrete volume of the specimen, V_c (mm^3)	Percentage of concrete replacement, V_r (%)
Ref.	Equation (1)	Equation (2)	Equation (3)	Equation (4)
CB1	0	84,000,000	84,000,000	0
PB1	5,166,000	84,000,000	78,834,000	6.2
PB2	8,496,000	84,000,000	75,504,000	10.1
PB3	11,526,000	84,000,000	72,474,000	13.7
PB4	5,664,000	84,000,000	78,336,000	6.7
PB5	11,328,000	84,000,000	72,672,000	13.5

Load-Displacement Response

Figure 3 and Figure 4 show the load-displacement responses of the specimens under flexural and shear loading. These curves reveal the structural behavior from the uncracked stage through yielding to final failure. Key properties such as first crack load, secant stiffness, yield load, and ultimate load were identified as in Table 9, with the yield point determined using the $0.75P_u$ criterion following [18]. This method was also adopted by [12] and [17].

The results are summarized in Table 10. All measurements were obtained from calibrated load cells and LVDTs. Readings were taken after holding the loads for at least one minute to allow stabilization. The smooth shape of the curves indicates that data noise was minimal, and its effect on comparative trends between specimens was considered negligible.

Three performance ratios were calculated: cracking load ratio (P_{cr}/P_u), yield load ratio (P_y/P_u), and ductility ratio (δ_u/δ_y) (Table 11). These ratios indicate the service load limit, strength reserve before failure, and ductility of the beams.

The first crack marks the end of uncracked elastic behavior and the start of visible cracking. The cracking load ratio (P_{cr}/P_u) shows how early cracking occurs relative to the beam's maximum strength. A higher ratio means better crack resistance. As shown in Table 11, beams with embedded polystyrene had lower cracking load ratios than conventional RC beams in both flexural and shear loading, indicating a lower threshold for initial cracking.

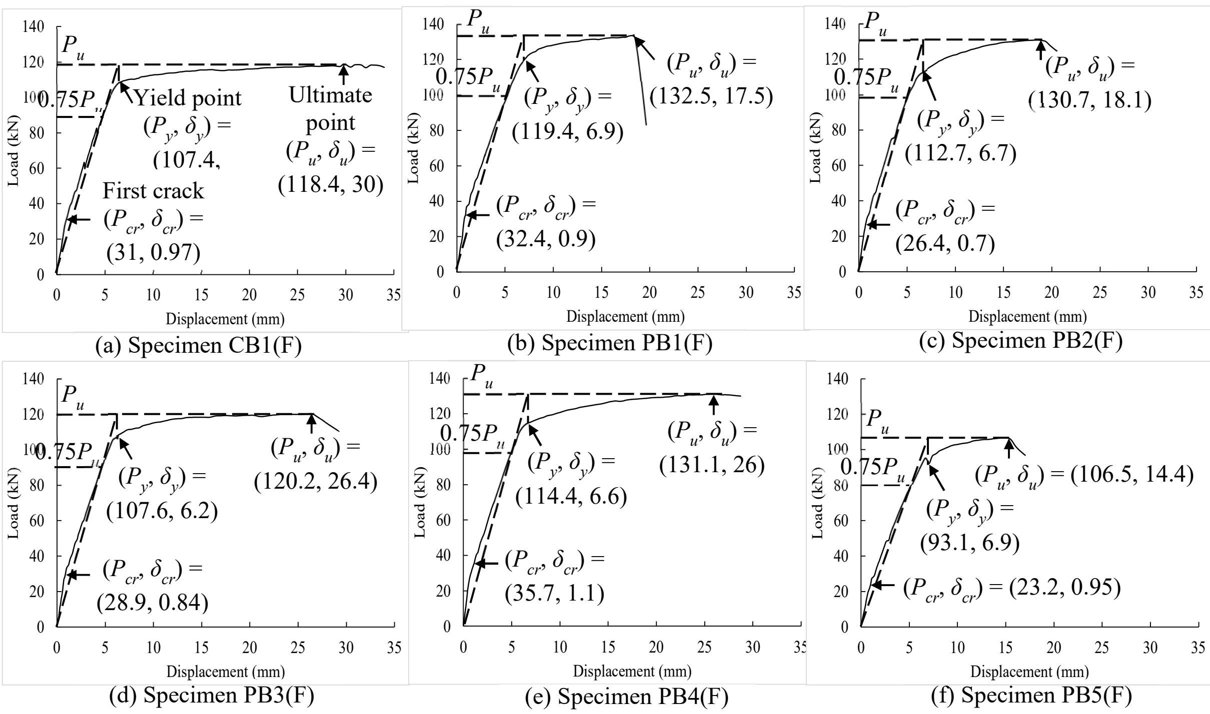

Figure 3. Load displacement response of specimens under flexural load

DOI: https://doi.org/10.35139/cantilever.v15i1.653

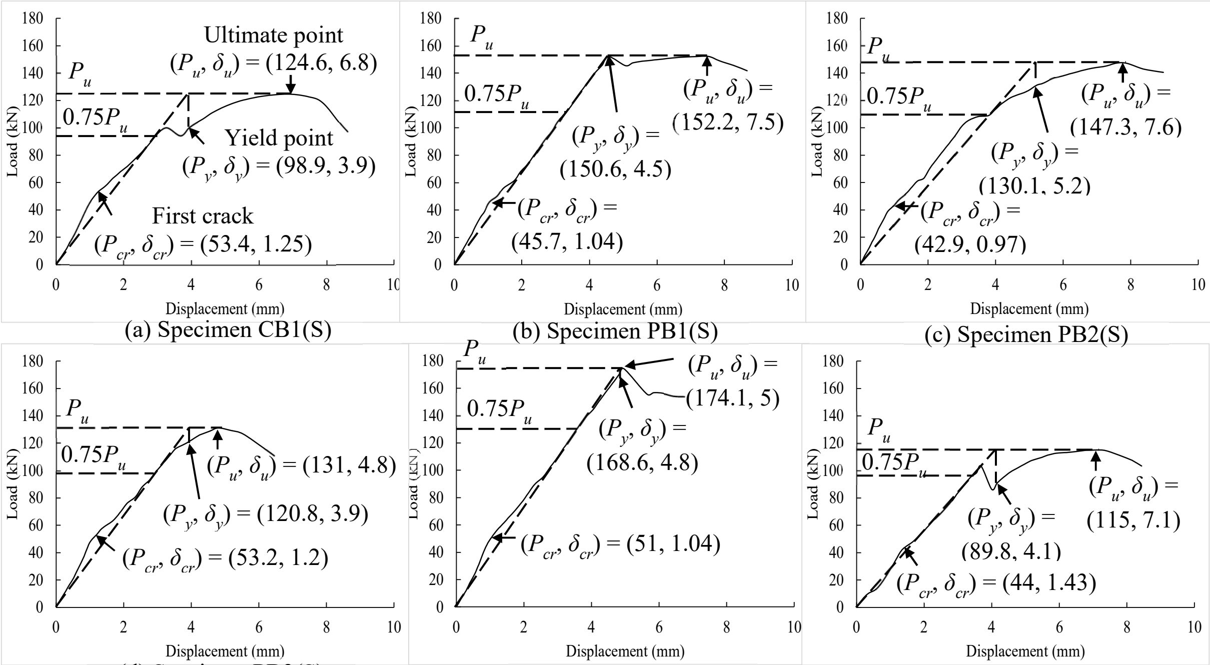

(a) Specimen CB1(S) (b) Specimen PB1(S) (c) Specimen PB2(S)
(d) Specimen PB3(S) (e) Specimen PB4(S) (f) Specimen PB5(S)

Figure 4. Load displacement response of specimens under shear load

Table 9. Specimen properties obtained from load-displacement response

Results	Description
First crack load, P_{cr}	The load when the first crack was noticed (Figure 5 and Figure 6).
First crack displacement, δ_{cr}	The beam deflection upon the first crack (Figure 3 and Figure 4).
Secant stiffness, S_s	The stiffness representing the pre-yield response of the specimen. It was taken as the slope of the line intercepting the point $0.75P_u$ (Figure 3 and Figure 4)
Yield point (P_y, δ_y)	The point marks the end of elastic deformation. It was determined using the $0.75P_u$ line following [18] (Figure 3 and Figure 4).
Ultimate load, P_u	The largest load sustained by the specimen (Figure 3 and Figure 4).
Ultimate displacement, δ_u	The deflection of the specimen at ultimate state (Figure 3 and Figure 4).

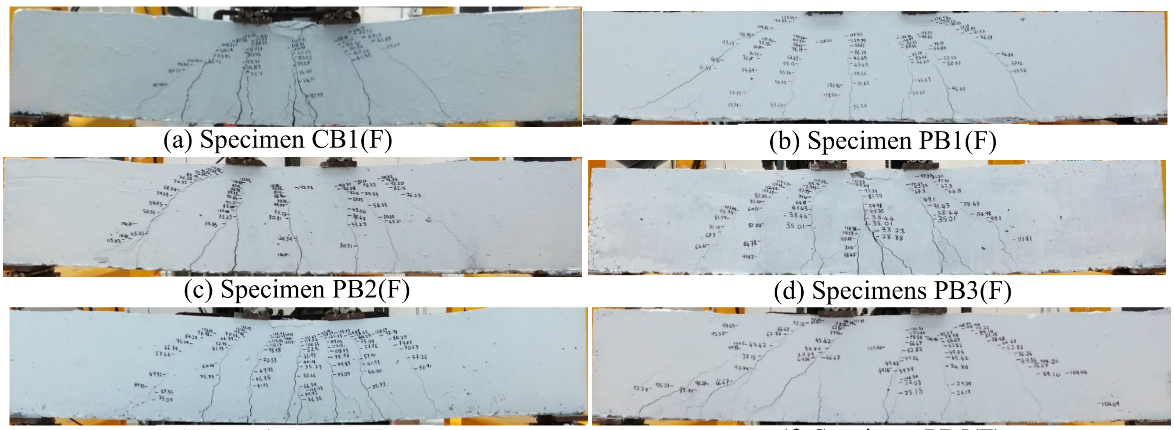

(a) Specimen CB1(F) (b) Specimen PB1(F)
(c) Specimen PB2(F) (d) Specimens PB3(F)
(e) Specimen PB4(F) (f) Specimen PB5(F)

Figure 5. Crack pattern of specimens under flexural load

DOI: https://doi.org/10.35139/cantilever.v15i1.653

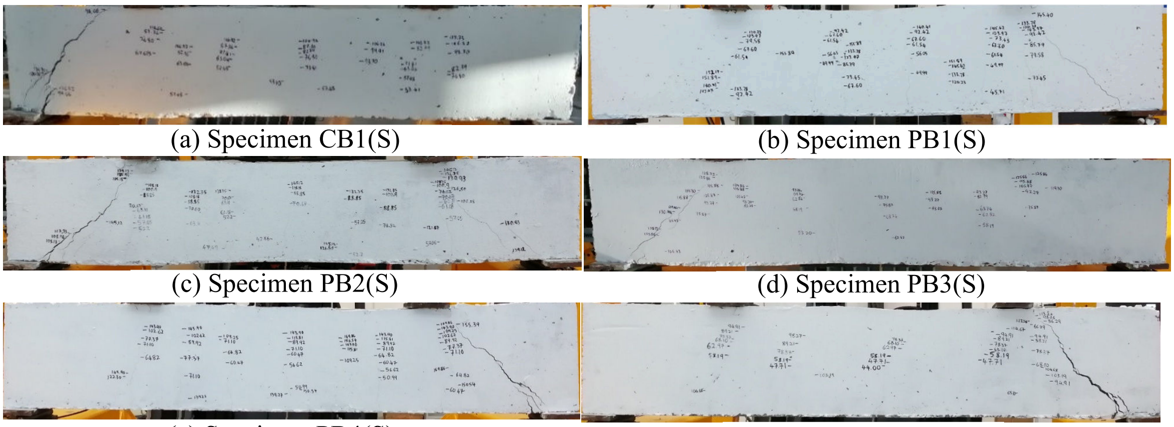

(a) Specimen CB1(S) (b) Specimen PB1(S)

(c) Specimen PB2(S) (d) Specimen PB3(S)

(e) Specimen PB4(S) (f) Specimen PB5(S)

Figure 6. Crack pattern of specimens under shear load

Table 10. Properties of specimens

Specimen	Secant stiffness (kN/mm)	First crack load, P_{cr} (kN)	Yield load, P_y (kN)	Yield displacement, δ_y (mm)	Ultimate load, P_u (kN)	Ultimate displacement, δ_u (mm)
CB1(F)	18.8	31.0	107.4	6.3	118.4	30.0
PB1(F)	19.1	32.4	119.4	6.9	132.5	17.5
PB2(F)	19.6	26.4	112.7	6.7	130.7	18.1
PB3(F)	19.3	28.9	107.6	6.2	120.2	26.4
PB4(F)	19.9	35.7	114.4	6.6	131.1	26.0
PB5(F)	15.4	23.2	93.1	6.9	106.5	14.4
CB1(S)	32.0	53.4	98.9	3.9	124.6	6.8
PB1(S)	33.6	45.7	150.6	4.5	152.2	7.5
PB2(S)	28.6	42.9	130.1	5.2	147.3	7.6
PB3(S)	33.5	53.2	120.8	3.9	131.0	4.8
PB4(S)	36.4	51.0	168.6	4.8	174.1	5.0
PB5(S)	27.9	44.0	89.8	4.1	115	7.1

Table 11. Performance ratio of the specimens

Specimen	Cracking Load Ratio, P_{cr}/P_u	Yield Load Ratio, P_y/P_u	Ductility ratio, δ_u/δ_y
CB1(F)	0.26	0.91	4.76
PB1(F)	0.24	0.90	2.54
PB2(F)	0.20	0.86	2.70
PB3(F)	0.24	0.90	4.26
PB4(F)	0.27	0.87	3.94
PB5(F)	0.22	0.87	2.09
CB1(S)	0.43	0.79	1.74
PB1(S)	0.30	0.99	1.67
PB2(S)	0.29	0.88	1.46
PB3(S)	0.41	0.92	1.23
PB4(S)	0.29	0.97	1.04
PB5(S)	0.38	0.78	1.73

A similar finding was reported by [4] and [14], where the first crack appeared earlier than in solid beams, typically at about one-quarter of the ultimate strength. [12] noted that replacing concrete with polystyrene changes the beam's geometry and stress distribution, causing higher stress near the soffit and larger strains that lead to early cracking. However, [2] found that increasing the distance between the polystyrene centroid and the soffit can delay crack formation.

The yield load marks the end of elastic behavior. The yield load ratio (P_y/P_u) indicates the strength margin from yield to failure. A lower ratio suggests a larger reserve for post-yield deformation and energy absorption. As shown in Table 11, beams with embedded polystyrene had lower yield load ratios under flexural loading but higher ratios under shear loading. This means they had better energy dissipation capacity under flexure than the conventional RC beam, which is useful for accidental or seismic events, but may have reduced reserve strength under shear, raising concerns about brittle failure.

The ductility ratio (δ_u/δ_y) indicates how much a beam deforms after yielding, with higher values showing better energy absorption. Table 11 shows that modified beams had lower ductility ratios under both flexural and shear loading, suggesting limited deformation and reduced resilience. Similar results were reported by [5, 12, 17]. The inclusion of

DOI: https://doi.org/10.35139/cantilever.v15i1.653

polystyrene disrupted the beam's section, leading to faster damage and earlier failure after yielding.

Overall, beams with embedded polystyrene showed inferior structural performance than conventional RC beams. The earlier onset of visible cracking indicates a reduced service load threshold under both flexural and shear loadings. While these beams demonstrated greater energy dissipation capacity under flexural loading, their performance under shear was less favorable, raising concerns about potential brittle failure in shear-dominant conditions. This issue could be mitigated by enhancing their shear reinforcement or using them in flexure-dominant settings. Additionally, the modified beams exhibited lower ductility than conventional beams under both loading modes, which may compromise their structural resilience under dynamic or extreme loading conditions.

Parametric Response

Among all specimens, only PB5 showed lower ultimate strength than the control beam (CB1). Although the use of a polystyrene block reduced concrete volume, it did not necessarily weaken the beam under flexural or shear loadings. PB5 had a 10% drop in flexural strength and 8% in shear strength, despite a 13.5% reduction in concrete volume, suggesting relatively efficient concrete use.

In comparison, specimen PB3 had a slightly higher concrete reduction (13.7%) but performed better, with a 2% increase in flexural strength and a 38% increase in shear strength. The key difference lies in the configuration of the polystyrene blocks. These results show that the shape and placement of the blocks within the beam cross-section are critical. A proper layout can enhance structural performance while reducing concrete usage.

Figure 7 shows that the geometry of the polystyrene section affects beam strength. Increasing the depth from 70 mm to 170 mm caused a gradual reduction in strength, with a 9% decrease in flexural strength and 14% in shear strength. Increasing the width from 40 mm to 80 mm had a greater effect, reducing flexural strength by 19% and shear strength by 34%. Both changes reduced concrete volume by a similar amount, around 7% to 8%, but increasing the width resulted in a more significant strength loss. This highlights the importance of polystyrene geometry, especially its layout within the beam cross-section, in influencing structural performance.

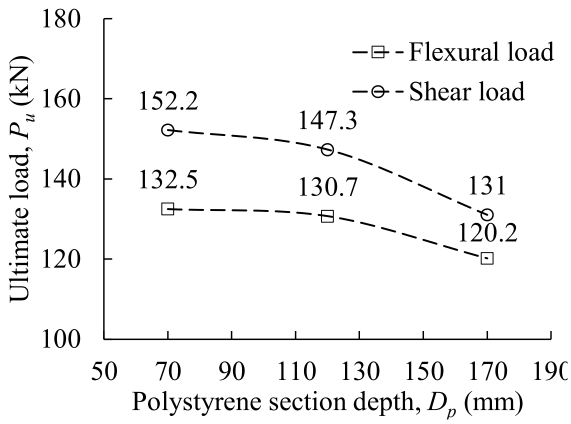

(a) Effects of polystyrene section depth

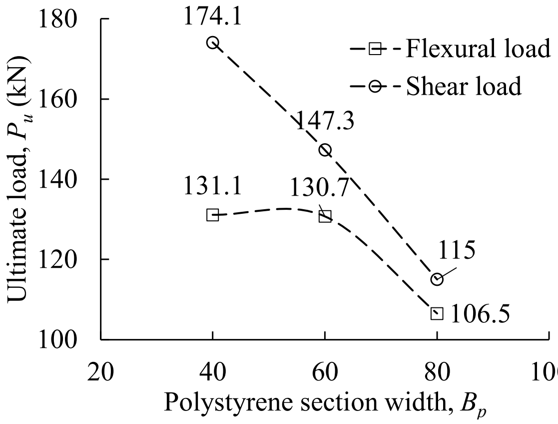

(b) Effects of polystyrene section width

Figure 7. Effects of polystyrene section depth and width on ultimate load of specimens

The beam's flexural capacity is linked to its effective moment of inertia (I_i) [12, 19], while shear capacity depends on the section area (A_i) [4]. To verify this, both properties were calculated based on the following assumptions:

1) For flexural loading, bending is dominant at mid-span under four-point loading, so I_i is calculated based on the mid-span cross section.
2) For shear loading, the critical section is located 263 mm (1d) from the support face, so A_i is taken from that cross section (Figure 8).
3) Polystyrene is treated as a void, as it offers minimal resistance to deformation [12].

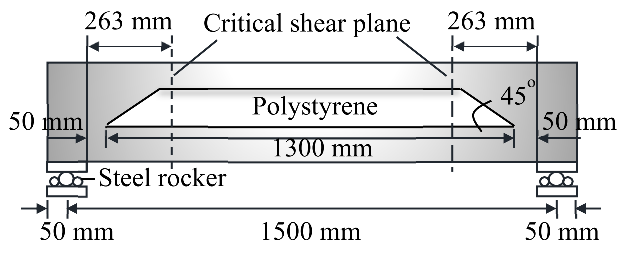

Figure 8. Critical shear plane of the specimen

Table 12 presents the calculated values, following the steps in Table 13. A plot of moment of inertia, I_i, versus flexural capacity and section area, A_i, versus shear capacity was then used to examine these relationships (Figure 9).

DOI: https://doi.org/10.35139/cantilever.v15i1.653

Table 12. Determining the moment of inertia of the specimen cross section

Specimen	A_p (mm²)	y_p (mm)	$\bar{y}$ (mm)	A_i (mm)	$d_{y,b}$ (mm)	$d_{y,p}$ (mm)	I_b (mm⁴)	I_p (mm⁴)	I_i (mm⁴)
CB1	0	0	150	52,500	0	-150	393,750,000	0	393,750,000
PB1	4,200	153	149.7	48,300	0.3	3.3	393,754,725	1,760,738	391,993,987
PB2	7,200	178	145.5	45,300	4.5	32.5	394,813,125	16,245,000	378,568,125
PB3	10,200	153	149.3	42,300	0.7	3.7	393,775,725	24,704,638	369,071,087
PB4	4,800	178	147.2	47,700	2.8	30.8	394,161,600	10,313,472	383,848,128
PB5	9,600	178	143.7	42,900	6.3	34.3	395,833,725	22,814,304	373,019,421

Notes:
Formula refer to Polystyrene section B_p, D_p and T_p refer to Table 1,
A_p = Area of polystyrene; y_p = Centroid of polystyrene; $\bar{y}$ = Beam centroid; A_i = Area of modified beam, $d_{y,b}$ = Centroid distance of solid beam; $d_{y,p}$ = Centroid distance of polystyrene; I_b = Moment of inertia of solid beam; I_p = Moment of inertia of polystyrene; I_i = Moment of inertia of modified beam

Table 13. Calculation to determine the moment of inertia of the section

	Solid beam	Polystyrene block	Modified beam
Area	A_b = 175 x 300 = 52,500 mm	$A_p = B_p D_p$	$A_i = A_b - A_p$
Centroid	y_b = 300 / 2 = 150 mm	$y_p = T_p + \frac{D_p}{2}$	$\bar{y} = \frac{A_b y_b - A_p y_p}{A_b - A_p}$
Centroid distance	$dy_b = \lvert y_b - \bar{y} \rvert$	$dy_p = \lvert y_p - \bar{y} \rvert$	
Moment of inertia	$I_b = \frac{175 \times 300^3}{12}$ =393,750,000	$I_b = \frac{B_p \times D_p{}^3}{12} + A_p dy_p{}^2$	$I = I_b - I_p$

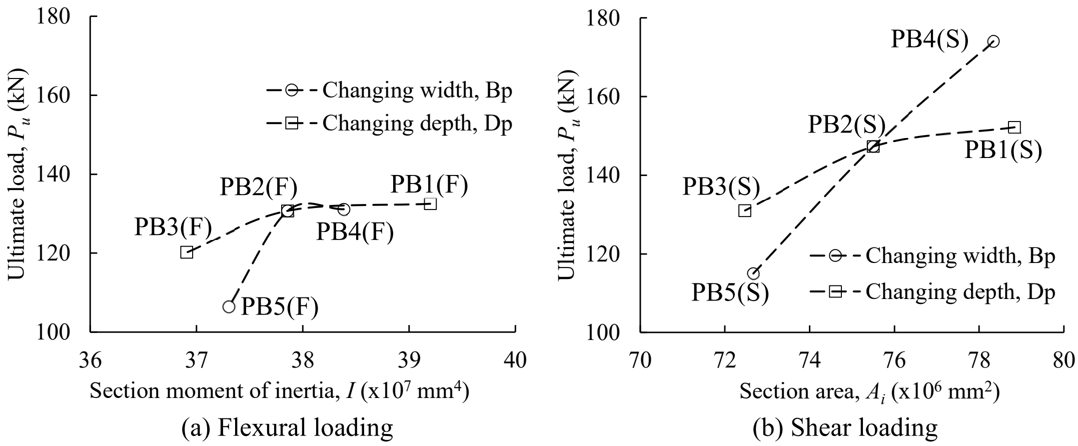

Figure 9. Effects of section moment of inertia and area on load-bearing capacity

Flexural load capacity was influenced by the moment of inertia (I_i), with ultimate load (P_u) generally increasing as I_i increased. Although the relationship was not perfectly proportional, P_u followed a consistent trend for PB3(F), PB2(F), PB4(F), and PB1(F) (Figure 9(a)). The variation in I_i was caused by changes in polystyrene width (B_p) and depth (D_p), yet the trend remained consistent. This suggests that I_i, which reflects bending resistance, has a stronger influence than the individual effects of B_p and D_p, indicating a clear direction for optimizing polystyrene design in the modified beam.

PB5(F), however, did not follow the trend (Figure 9), suggesting other factors influenced its performance. Although depth (D_p) theoretically has a stronger cubic influence on moment of inertia, the experimental trend shows width (B_p) can dominate within the tested range due to its effect on concrete cover and bond with the reinforcement.

One likely reason is the polystyrene layout, which reduced the concrete surrounding the tension bar and shear link, as shown in Figure 10. The clear distance between the tension bar and polystyrene was 19 mm, and 16.5 mm for the shear link. Both were less than the 25 mm nominal concrete cover, which may have weakened the bond between the bars and the concrete. [4] stated that insufficient cover caused by polystyrene can reduce bond strength, alter stress and strain behavior, affect creep resistance, and lower the overall performance.

DOI: https://doi.org/10.35139/cantilever.v15i1.653

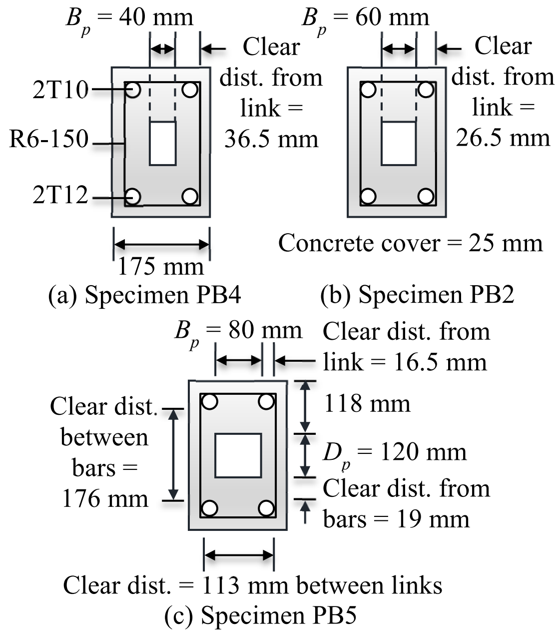

Figure 10. Clear distance between polystyrene section and reinforcements of specimen PB4, PB2, and PB5

Concrete around reinforcement is essential for stress transfer through adhesion, friction, and mechanical interlock, contributing to bond strength. It also supports the overall stiffness and integrity of the beam. When this concrete is reduced, bond strength declines, increasing the risk of bar slip and reducing the effectiveness of both tension and shear reinforcement. This limits the beam's ability to reach its full flexural capacity and likely explains the lower performance of PB5(F) compared to the other specimens.

A higher moment of inertia increases a beam's flexural stiffness, reducing deflection under load. While this concept is straightforward for homogeneous materials like steel, it also applies to RC beams using transformed sections. In RC beams, flexural capacity depends on internal forces: the tensile force in the steel and the compressive force in the concrete, multiplied by their lever arm. With only 0.4% tension reinforcement, the beam is under-reinforced, and strength is primarily limited by the steel. The section geometry still plays a role, affecting the lever arm and stiffness, which may explain the observed correlation between flexural capacity and moment of inertia. However, since the moment of inertia is not the direct source of flexural resistance, the relationship is not linear.

Figure 9(b) shows the relationship between ultimate shear capacity (P_u) and section area (A_i). P_u generally increases with A_i, indicating a positive correlation. Variations in width (B_p) and depth (D_p) affect P_u at different rates, with B_p having a stronger influence, as reflected by its stiffer gradient. The B_p trend line (PB5(S), PB2(S), PB4(S)) is more linear, while the D_p trend line (PB3(S), PB2(S), PB1(S)) appears parabolic. This suggests that B_p has a greater and more consistent effect on shear capacity than D_p.

Theoretically, beam shear resistance depends on both concrete and shear reinforcement. Polystyrene acts as a void, reducing the effective concrete area (A_i). This reduction in A_i explains the decrease in shear capacity (P_u) observed with both B_p and D_p variations.

Increasing B_p reduces the concrete cover between the polystyrene and shear links. In PB4, PB2, and PB5, the clear distances were 36.5 mm, 26.5 mm, and 16.5 mm, respectively (Figure 10). PB5 fell below the nominal 25 mm cover, potentially weakening the bond and lowering shear resistance. In contrast, increasing D_p did not reduce the cover below the nominal value. PB3 had the smallest distances of 37 mm (top), 31 mm (bottom), and 26.5 mm (side) (Figure 11). This suggests B_p has a greater impact on shear capacity than D_p.

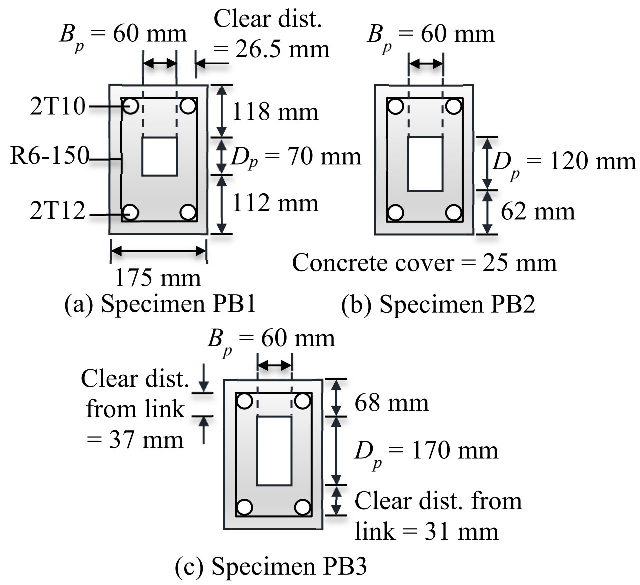

Figure 11. Clear distance between polystyrene section and shear links of specimens PB1, PB2 and PB3

Efficiency Analysis

The efficiency of a specimen can be quantified using the efficiency ratio, R_e, defined as:

$$R_e = \frac{R_s}{R_v} \quad (5)$$

where R_s is the strength ratio, and R_v is the volume ratio.

This ratio compares the change in structural strength relative to the change in concrete volume. A value of R_e more than 1.0 is desirable, as it indicates that the specimen either gained strength despite a reduction in concrete volume or lost less strength than the amount of volume reduced; resulting in a higher strength-to-concrete ratio compared to the solid beam.

DOI: https://doi.org/10.35139/cantilever.v15i1.653

The strength ratio, R_s, is calculated as:

$$R_s = \frac{P_{u,i}}{P_{u,c}} \quad (6)$$

where $P_{u,i}$ is the ultimate load capacity of the specimen (kN), and $P_{u,c}$ is the ultimate load capacity of the control beam (CB1(F) for flexural tests and CB1(S) for shear tests) (kN).

The volume ratio, R_v, represents the remaining concrete volume relative to the original solid beam and is calculated as:

$$R_v = \frac{V_c}{V_b} \quad (7)$$

where V_c is the concrete volume of the specimen, and V_b is the volume of the solid control beam.

Table 14 presents the strength ratio (R_s), volume ratio (R_v), and efficiency ratio (R_e) of the specimens under both flexural and shear loadings.

Table 14. Efficiency ratio of specimen

Specimen	Strength ratio, R_s	Volume ratio, R_v	Efficiency ratio, R_e
Ref.	Equation (6)	Equation (7)	Equation (5)
PB1(F)	1.12	0.94	1.19
PB2(F)	1.10	0.90	1.22
PB3(F)	1.02	0.86	1.19
PB4(F)	1.11	0.93	1.19
PB5(F)	0.90	0.87	1.03
PB1(S)	1.22	0.94	1.30
PB2(S)	1.18	0.90	1.31
PB3(S)	1.05	0.86	1.22
PB4(S)	1.40	0.93	1.51
PB5(S)	0.92	0.87	1.06

Under flexural loading, all specimens had efficiency ratios (R_e) above 1.0, showing improved material use despite reduced concrete volume. PB2(F) had the highest R_e of 1.22, with a 10% strength gain and 10% volume reduction. PB1(F), PB3(F), and PB4(F) followed closely with similar R_e values around 1.19, showing consistent and favorable efficiency across those configurations. PB5(F), despite a 10% strength loss, had a 13% volume reduction, resulting in a lower R_e of 1.03. Although slightly better than the control, it was the least efficient among the modified beams.

Under shear loading, all specimens again showed R_e values above 1.0. PB4(S) was the most efficient at 1.51, gaining 40% in strength while keeping 93% of its volume. PB2(S), PB1(S), and PB3(S) followed with R_e values of 1.31, 1.30, and 1.22. PB5(S) had the lowest efficiency at 1.06, due to limited strength gain and moderate volume reduction, likely caused by a less effective polystyrene layout.

Efficiency varied more under shear than flexural loading, indicating that polystyrene configuration has a greater impact under shear-dominated conditions. PB2 was the most efficient in flexure, while PB4 led in shear. However, for lightweight design goals, PB2 is more favorable as it replaced more concrete (10%) than PB4 (7%), achieving both strength efficiency and greater weight savings.

Despite the favorable efficiency ratios, strength-based efficiency alone does not fully represent structural performance. The yield load ratio (P_y/P_u) and ductility ratio (δ_u/δ_y) discussed previously must also be considered to ensure that reductions in concrete volume do not compromise safety or deformation capacity. For consistency within the efficiency-based evaluation framework, they are herein expressed as the serviceability ratio (R_{sv}) and ductility ratio (R_d), respectively.

The serviceability ratio, R_{sv}, reflects the available post-yield reserve before failure. Following [12, 17] and adopting the recommendation in [22, 23], a minimum value of $R_{sv} \geq 0.75$ is considered acceptable to ensure sufficient reserve strength beyond yielding.

From Table 11, R_{sv} ranged from 0.78 to 0.99, satisfying the minimum requirement. However, PB1(S), PB3(S), and PB4(S) recorded relatively high values of 0.99, 0.92, and 0.97, respectively. Ratios approaching unity indicate that yielding occurs close to ultimate capacity, leaving limited post-yield strength reserve. While still above the minimum threshold, such high values may reduce tolerance to underestimation of loads or unexpected overloads.

Previous studies [12, 17, 22, 23] reported R_{sv} values generally below 0.90. In this context, an upper practical limit of approximately 0.90 may be considered reasonable to ensure adequate post-yield reserve. Based on this criterion, PB1(S), PB3(S), and PB4(S) exhibit comparatively limited reserve capacity.

Ductility is another critical parameter influencing structural safety, particularly under dynamic or seismic loading. For low to moderate seismic regions, a minimum R_d of 4.0 is commonly recommended [22, 23] to ensure sufficient deformation capacity prior to failure.

From Table 11, only CB1(F) and PB3(F) achieved $R_d \geq 4.0$ under flexural loading, while PB4(F) was marginal at 3.94. The remaining flexural specimens exhibited lower ductility, indicating reduced deformation capacity after yielding. Under shear loading, none of the specimens, including CB1(S), satisfied the $R_d \geq 4.0$ criterion. This confirms that shear-dominant behavior results in limited ductility and underscores the importance of preventing shear-controlled failure through adequate shear reinforcement.

Overall, although the modified beams demonstrate favorable strength-to-volume efficiency and meet the minimum serviceability requirement, certain configurations exhibit limited post-yield

DOI: https://doi.org/10.35139/cantilever.v15i1.653

reserve and reduced ductility. Therefore, optimization of polystyrene geometry should balance material efficiency with adequate deformation capacity to ensure both economic and structural performance.

Limitations

The strength ratio was determined based on the measured ultimate load capacity. Although all specimens used the same nominal grade Y12 reinforcing steel, the reported variability in the mechanical properties of the reinforcement may introduce uncertainty in flexural capacity despite identical reinforcement detailing.

The interpretation of strength enhancement and efficiency in this study, as reflected by the strength ratio R_s and efficiency ratio R_e, assumes that this variability has limited influence. All specimens exhibited significant cracking and large deformation at failure, consistent with yielding behavior of the tensile reinforcement, bond degradation, and progressive loss of structural integrity. No tensile fracture of the steel bars was observed at the ultimate state, indicating that failure was governed by deformation and bond deterioration rather than rupture of the reinforcement.

Nevertheless, the exact contribution of reinforcement strength variability to the measured flexural capacity cannot be quantified within the current experimental framework, particularly because strain gauges were not installed on the reinforcement and the yield strength of the steel bars was not experimentally determined. This remains a limitation of the study.

Also, each beam configuration was tested using a single specimen without replication. While the observed behavioral trends were consistent across the tested specimens, the absence of repeated specimens limits statistical validation and prevents quantitative assessment of experimental variability. As a result, the reported strength, efficiency, serviceability, and ductility ratios (i.e., R_s, R_e, R_{sv}, and R_d) should be interpreted as indicative rather than statistically definitive. Future work should include replicated specimens to improve reliability and enable statistical evaluation of performance consistency.

In addition to experimental constraints, the modified beam also faces practical limitations, particularly in constructability. Polystyrene must be precisely positioned within the formwork and reinforcement cage to maintain structural geometry. Large blocks like those used in this study require horizontal insertion into the cage before formwork placement, complicating the work sequence. Due to their light weight and buoyancy, these blocks may shift or float during concreting if not securely anchored, leading to delays and increased labor requirements. Polystyrene also reduces the space available for concrete flow and compaction, increasing the risk of honeycombing and voids, which may compromise structural integrity.

In comparison, the use of voids or lightweight materials in slabs has gained wider acceptance. Achieving a similar level of acceptance in beams is more difficult due to the greater complexity of replacing concrete, as beams typically have smaller cross-sectional areas and denser reinforcement than slabs. Structurally, modified beams are also less appealing. According to [6], lightweight slabs are more efficient than beams, offering a higher percentage of weight reduction relative to strength loss. [17] further support this, reporting that while polystyrene spheres performed well in slabs, their use in beams led to a 2% to 4% decline in material efficiency and a 7% to 14% reduction in load capacity.

Furthermore, polystyrene is a thermoplastic material that is highly combustible [20]. Under high temperatures, it melts and ignites, releasing dense black smoke and toxic fumes [21], which hinder evacuation and rescue efforts. Structurally, its presence accelerates internal temperature rise, potentially leading to faster heat transfer to reinforcement. This compromises the beam's load-carrying capacity and reduces its fire resistance compared to conventional solid beams. As a result, such beams may not meet fire rating requirements for many structural applications. While external fireproofing can offer some protection, the flammability of the core remains a critical limitation under prolonged fire exposure.

Despite these limitations, the study's contribution extends beyond the practical challenges of embedding polystyrene. It clarifies how internal void configurations affect the flexural and shear behavior of RC beams. Although polystyrene may not be suitable for conventional construction, the structural insights gained can support future systems that incorporate intentional voids using more appropriate materials or advanced fabrication methods such as 3D printed concrete. This positions the work as a foundation for developing optimized lightweight beam systems rather than merely evaluating polystyrene inclusion.

4. CONCLUSION

This study examined the structural performance of RC beams embedded with trapezoidal polystyrene under flexural and shear loading. Results show that polystyrene can be incorporated without compromising load-bearing capacity. The geometry of embedded polystyrene affects beam performance.

DOI: https://doi.org/10.35139/cantilever.v15i1.653

Increasing the width reduces flexural and shear capacity more than increasing the depth. This is mainly due to the reduced moment of inertia and concrete area, though poor concrete cover and weak bond strength may also contribute.

Specimen PB2 showed the best performance, with 22% and 31% higher material efficiency than solid beams in flexural and shear loading, respectively, at 10% concrete replacement. This was due to a 10% increase in flexural capacity and an 18% increase in shear capacity. However, these gains came with lower cracking resistance and reduced ductility under both loading conditions.

Despite its potential, practical challenges remain. The construction process is more complex and labor-intensive, and the combustibility of polystyrene raises fire safety concerns. Addressing these issues is essential before this method can be widely adopted in structural applications.

The findings are based on laboratory-scale testing with a limited number of specimens; therefore, generalization to full-scale structural applications should be made with caution.

ACKNOWLEDGEMENTS

This research work was funded by the Research Grants of University of Technology Sarawak UCTS/RESEARCH/2/2018/02.

REFERENCES

[1] J.H. Ling, J.T.S. Ngu, Y.T. Lim, W.K. Leong, H.T. Sia, “Experimental study of RC hollow beams with embedded PVC pipes,” *Journal of Advanced Civil and Environmental Engineering*, vol. 5, no. 1, pp. 11–23, 2022, doi: 10.30659/jacee.5.1.11-23.

[2] Y.T. Lim, J.H. Ling, J.W. Lau, T.T.L. Danson, “Performance of reinforced concrete beam with polystyrene blocks at various regions,” *Journal of Science and Applied Engineering*, vol. 3, no. 2, pp. 62–71, 2021, doi: 10.31328/jsae.v3i2.1655.

[3] Y.T. Lim, J.H. Ling, H.T. Sia, L.W. Kam, J.T.S. Ngu, “Improvement in the reinforced concrete beam with embedded polystyrene under static load,” *Indonesian Journal of Computing, Engineering, and Design*, vol. 5, no. 2, pp. 67–77, 2023, doi: 10.35806/ijoced.v5i2.331.

[4] J.W. Lau, J.H. Ling, Y.T. Lim, “Feasibility study of reinforced concrete beam with embedded polystyrene spheres under incremental flexural load,” *Borneo Journal of Science and Technology*, vol. 2, no. 2, pp. 11–26, 2020. [Online]. Available: https://journal.uts.edu.my/Home/ArticleDownload?articleId=BJOST020204

[5] Y.T. Lim, J.H. Ling, J.W. Lau, A.Y.M. Yik, “Experimental study on the flexural behavior of reinforced polystyrene blocks in concrete beams,” *Journal of the Civil Engineering Forum*, vol. 7, no. 2, pp. 197–208, 2021, doi: 10.22146/jcef.62346.

[6] Y.T. Lim, J.H. Ling, “Incorporating lightweight materials in reinforced concrete beams and slabs – A review,” *Borneo Journal of Sciences and Technology*, vol. 1, no. 2, pp. 16–26, 2019. [Online]. Available: https://journal.uts.edu.my/Home/ArticleDownload?articleId=BJOST010203

[7] L. Ragavi, “Behaviour of reinforced concrete hollow beams under monotonic loading,” *World Journal of Technology, Engineering and Research*, vol. 2, no. 1, pp. 127–136, 2017.

[8] A.J.H. Alshimmeri, H.N.G. Al-Maliki, “Structural behavior of reinforced concrete hollow beams under partial uniformly distributed load,” *Journal of Engineering*, vol. 20, no. 7, pp. 130–145, 2014, doi: 10.31026/j.eng.2014.07.09.

[9] T.S. Al-Gasham, A.N. Hilo, M.A. Alawsi, “Structural behavior of reinforced concrete one-way slabs voided by polystyrene balls,” *Case Studies in Construction Materials*, vol. 11, pp. 1–13, 2019, doi: 10.1016/j.cscm.2019.e00292.

[10] S. Inoue, N. Egawa, “Flexural and shear behaviour of reinforced concrete hollow beams under reversed cyclic loads,” in Proc. *Eleventh World Conference on Earthquake Engineering*, 1996.

[11] T.S.S. Al-Gasham, “Reinforced concrete moderate deep beams with embedded PVC pipes,” *Wasit Journal of Engineering Science*, vol. 3, no. 1, pp. 19–28, 2015, doi: 10.31185/ejuow.Vol3.Iss1.32.

[12] J.H. Ling, J.W. Lau, Y.T. Lim, “Structural behaviour of reinforced concrete beam with embedded polystyrene spheres,” *Civil and Sustainable Urban Engineering*, vol. 3, no. 1, pp. 25–39, 2023, doi: 10.53623/csue.v3i1.180.

[13] D.T.L. Tan, J.H. Ling, “Flexural behaviour of reinforced concrete beam embedded with different alignment of polystyrene,” *Borneo Journal of Sciences and Technology*, vol. 2, no. 1, pp. 13–18, 2019. [Online]. Available: https://journal.uts.edu.my/Home/ArticleDownload?articleId=BJOST020104

[14] N. Mohamad, W.I. Goh, A.A.A. Samad, A. Lockman, A. Alalwani, “Structural behaviour of beam with HDPE plastic balls subjected to flexural load,” *Materials Science Forum*, vol. 889, pp. 270–274, 2017, doi: 10.4028/www.scientific.net/MSF.889.270

[15] B. Mosley, J. Bungey, R. Hulse, *Reinforced Concrete Design to Eurocode 2*, 7th ed., Palgrave Macmillan, England, 2012.

[16] British Standard, Eurocode 2: Design of Concrete Structures – Part 1-1: General Rules and Rules for Buildings, BS-EN 1992-1-1:2004, 2004.

[17] J.H. Ling, J.W. Lau, Y.T. Lim, “Behaviour of RC beam-slab member with embedded polystyrene spheres,” *Journal of Civil Engineering*, vol. 40, no. 1, pp. 3–11, 2025, doi: 10.12962/j20861206.v40i1.19650.

[18] R. Park, “Ductility evaluation from laboratory and analytical testing,” in Proc. *Ninth World Conference on Earthquake Engineering*, Tokyo-Kyoto, Japan, 1988, pp. 605–616. [Online]. Available: https://www.iitk.ac.in/nicee/wcee/article/9_vol8_605.pdf

[19] C. Bailey, T. Bull, A. Lawrence, “The bending of beams and the second moment of area,” *The Plymouth Student Scientist*, vol. 6, no. 2, pp. 328–339, 2013, doi: 10.24382/8z3x-cx21.

[20] M. Qin, X. Hu, J. Guo, “Preparation of a new type of expansion flame retardant and application in polystyrene,” *Coatings*, vol. 13, no. 4, pp. 733, 2023, doi: 10.3390/coatings13040733.

[21] J.L. Gurman, L. Baier, B.C. Levin, “Polystyrenes: A review of the literature on the products of thermal decomposition and toxicity,” *Fire and Materials*, vol. 11, no. 3, pp. 109–130, 1987, doi: 10.1002/fam.810110302.

[22] J.H. Ling, A.B. Abd. Rahman, I.S. Ibrahim, Z. Abdul Hamid, “An experimental study of welded bar sleeve wall panel connection under tensile, shear, and flexural loads,” *International Journal of Concrete Structures and Materials*,

DOI: https://doi.org/10.35139/cantilever.v15i1.653

vol. 11, pp/ 525–540, 2017, doi: 10.1007/s40069-017-0202-y.

[23] J.H. Ling, A.B. Abd. Rahman, I.S. Ibrahim, “Deformation behavior of grouted sleeve wall connector under shear load in precast process of concrete wall.” *Indonesian Journal of Computing, Engineering, and Design*, vol. 4, pp. 1–14, (2022), doi: 10.35806/ijoced.v4i2.263.

DOI: https://doi.org/10.35139/cantilever.v15i1.653